Chalcogenide Letters Vol. 18, No. 5, May 2021, p. 225 - 235

Construction and tribological behaviors of MXenes/MoS_2 heterojunction with 2D/2D structure in liquid paraffin

F. X. Zhang[a*], X. Su[b], G. G. Tang[a], J. Xu[b,*]
[a]*School of Modern Equipment Manufacturing, Zhenjiang College, Zhenjiang, Jiangsu province 212028, P. R. China*
[b]*School of physics and electrical engineering, Jiangsu University, Zhenjiang, Jiangsu province 212013, P. R. China*

In this work, novel MXenes/MoS_2 heterojunction of flower-like MoS_2 decorated sheet-like MXenes were successfully fabricated by one-step hydrothermal approach using TiO_2 as the precursor, and systematically investigated by a series of characterizations (e.g. XRD, Raman, SEM, and TEM analysis). Furthermore, the tribological behaviour of MXenes/MoS_2 heterojunction in liquid paraffin were extensively examined a ball-on-disk tribometer. The effects of applied load and rotational speed were also investigated. The experimental results indicated the friction and wear was significant decreased with introduction of MXenes/MoS_2 heterojunction. Especially, 5%-MXenes/MoS_2-paraffin samples show the lowest friction coefficient (~0.10). Additionally, the construction and excellent tribological properties of MXenes/MoS_2 heterojunction would be beneficial for the design of novel nano-additives with 2D/2D structure for enhancing friction reduction and anti-wear, which also would expand their actual applications in the industry and agriculture.

(Received March 7, 2021; Accepted May 3, 2021)

Keywords: MoS_2, MXenes, Heterojunction, 2D/2D structure, Tribological properties

1. Introduction

As we know, friction is universal in modern industry. Without friction, all mechanical components cannot work [1-3]. Furthermore, friction and wear are the major causes for the loss in materials and energies [4-6]. Generally, lubricants have been considered the most effective approach to reduce friction and wear, and prolong the service life of machines for energy loss [7-10]. Recently, many inorganic nanoparticles have been widely concerned as the promising and potential lubricant due to their excellent friction-reducing and anti-wear performances [11-14]. Therefore, exploring and developing novel inorganic nanoparticles or their composites for enhancing their tribological properties is the biggest challenge at present [15-18].

Nowadays, two-dimensional (2D) layered materials, like graphene and MoS_2, have gained considerable attention in the search for novel nano-lubricants to reducing friction and wear because their lamellar structures and easy interlayer sliding ascribed to the weak van der Waals

* Corresponding author: xjing@ujs.edu.cn
https://doi.org/10.15251/CL.2021.185.225

interactions within their molecular layers [19-22]. In the characteristic layered structure of MoS_2, a Mo atomic layer sandwiched two S atomic layers. And the intralaminar of S–Mo–S layer is strong covalent, while the interlayer of sandwiched structure is weak Van der Waals force, resulting the decrease in friction coefficient and possess enhanced reducing-friction and anti-wear properties [23-26]. More importantly, nano-sized MoS_2 show more excellent tribological properties compared to commercial MoS_2, which can be applied in harsh working environments, e.g. high pressure and high vacuum [27]. Recently, many previous researches indicated the modification of micro/nano-scale MoS_2 with introduction of other semiconductor nanoparticles can further improve its anti-friction and wear resistance [28-30]. Thus, MoS_2-incorporated composites composed of MoS_2 and other nanomaterials (e.g. graphene, WS_2, MoO_3 and h-BN, etc.) have been received extensive attention and synthesized through various methods, which also exhibited reinforcing and lubricating effects compared to that of pure MoS_2 [31-35].

Currently, MXenes, a novel 2D lamellar material, have attracted considerable attention and widely applied in lithium-ion batteries, super capacitors, heavy metal adsorption, and photocatalytic or electrocatalytic H_2 evolution because of graphene-like structure, hydrophilic surfaces, chemical stability, and outstanding electrical conductivities [36-38]. Furthermore, MXenes possess superior frictional properties and self-lubricating performance owing to its unique lamellar structure, high mechanical strength and low shear strength [39]. As expected, MXenes and its composites have been utilized as solid lubricant or lubricating additive for improving tribological properties. However, the construction and macro-scale tribological properties of MXenes/MoS_2 using as a lubricating additive have not been reported yet.

Herein, novel 2D/2D MXenes/MoS_2 heterojunction were constructed and synthesized by one-step hydrothermal approach using MXenes as the precursor. And their frictional and wear behaviors were comparatively investigated by a ball-on-disk tribometer. Furthermore, the morphology and composition of the wear tracks were characterized by SEM, SMP and EDX technologies, which were conducted to understand their friction and wear mechanisms. Thus the construction and excellent tribological properties of MXenes/MoS_2 heterojunction would be beneficial for the design of novel nano-additives with 2D/2D structure for enhancing friction reduction and anti-wear, which also would expand their actual applications in the industry and agriculture.

2. Experimental section

2.1. Synthesis of MXenes nanosheets

The MXenes nanosheets were synthesized by etching Al from Ti_3AlC_2 in HF solution. Typically, Ti_3AlC_2 (5g) powders was immersed in HF solution (50 mL, 40%) for continuous stirring for 24 h at room temperature. After that, the as-prepared MXenes powder were obtained after repeated washings with DI water and ethanol to neutral, then drying at 80 ˚C in a vacuum oven for 8 h.

2.2. Synthesis of MXenes/MoS_2 heterojunction

MXenes/MoS_2 heterojunction were fabricated by one-step hydrothermal approach u in the presence of MXenes. A certain amount of in the presence of sheet-like MXenes were added to 30

mL deionized water and continuous ultra-sonicated for 1 h. Then, $(NH_4)_2MoO_4 \cdot 4H_2O$ (0.8 g) and CH_4N_2S (3.6 g) were mixed with the above sonic solution, successively; and Polyvinylpyrrolidone (PVP) is used as a surfactant, which addition amount is 2.2 g. After strong agitation for 1h, the above suspension was subsequently transferred into a 50 mL Teflon-lined stainless steel autoclave and maintained at 180 ℃ for 24 h. Finally, MXenes/MoS_2 samples with various concentrations of MXenes were obtained after repeated washings with DI water and ethanol and drying at 60 ˚C in a vacuum oven for 8 h, which also was labeled as MM-1, MM-2, MM-3, MM-4, MM-5, and the addition amount of MXenes is 5%, 10%, 15%, 20%, 30%, respectively. Additionally, pure MoS_2 were prepared by the similar hydrothermal approach without the addition of MXenes.

2.3. Characterization

XRD (Bruker-AXS), XPS (Thermo Scientific K-Alpha+ system), Raman Microscope (DXR-Thermo Scientific), SEM (JEOL JXA-840A) and TEM analysis (JEOL JEM-2100) are performed to investigate the phase compositions, chemical states and microstructure of the as-prepared products.

2.4. Tribological test

The friction reduction and anti-wear of pure base oil contained various nano-additives was investigated by a ball-on-disk tribometer (MS-T3001, China). In our experiments, liquid paraffin was selected as the lubricating oil. During experiments, the rotary velocity of the steel ball was kept 200 rpm, and the applied load was set to 2 N for 0.5 h at room temperature. Also, different tribological variables including the additive concentration (0.7-7 wt %), rotary velocity (100-500 rpm), and applied load (2-6 N) were investigated. More importantly, all friction experiments were investigated three times, respectively. Afterwards, the surface roughness and elemental composition of the worn surfaces were quantified by non-contact optical 3D profilers (SMP, NT1100, Veeco WYKO, USA), Atomic Force Microscopy (AFM, MFP-3D, USA), and SEM-EDS analysis (HITACHI S-3400N, Japan).

3. Results and discussion

The phase structure and crystallization of pure MoS_2, MXene and MoS_2/MXene composites were investigated by XRD technology, resulted in Fig. 1. For pure MoS_2, The characteristic peaks located at 17.26°, 32.46°, and 57.9° can be indexed to the typical (002), (100) and (110) planes of MoS_2 (JCPDS no. 37-1492) [40,41], and the diffraction peaks appearing at 18.02°, 27.46°, 36.02°, 41.82°and 60.64° is consistent with the (004), (006), (101), (105) and (110) planes of Ti_3C_2 MXenes (JCPDS No. 32-1383) [42]. Compared with pure MoS_2, the peak position and intensity of the MoS_2/MXene composites do not change obviously with the introduction of MXene, possibly due to the low content of MXene. With the increasing MXene content (MXene/MoS_2-0.15), the diffraction peaks of MXene tended to be apparent gradually, implying the successful interaction of MoS_2 nanosheets in MXene layers. Furthermore, Raman spectra was employed to detect the presence of MXene and MoS_2, and resulted in Fig. 2. Obviously, the Raman peaks located at 1363 cm^{-1} and 1557 cm^{-1}, which are consistent with to D band and G band of carbon atoms. And the band at 185, 250, 414, and 605 cm^{-1} are well correlated with

vibrations originating from $Ti_3C_2O_2$, $Ti_3C_2F_2$ and $Ti_3C_2(OH)_2$ [43,44]. For pure MoS_2, the Raman band located at 361.2 and 402.6 cm^{-1} corresponding to its E^1_{2g} and A_{1g} modes [40]. Additionally, the characteristic bands positions of MXene and MoS_2 were coexisted in the compositesamples, indicating the successful construction of MXenes/MoS_2 heterojunction.

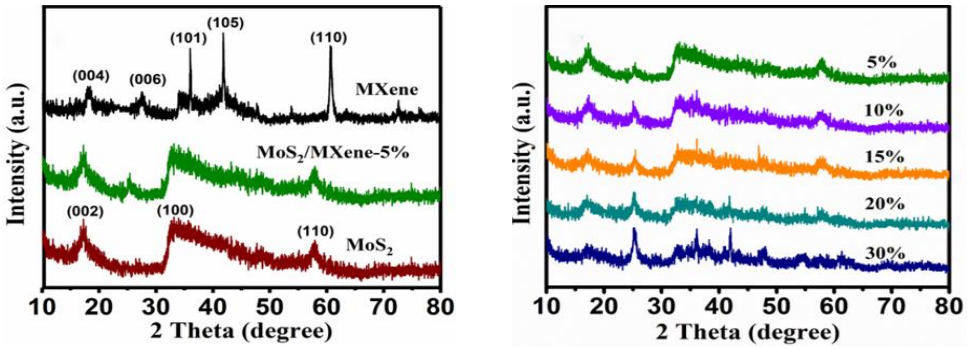

(a) *(b)*

Fig. 1. (a) XRD patterns of MXene, MoS_2 and MoS_2/MXene-5% composites; (b) XRD patterns of MoS_2/MXene composites with different amounts of MXene.

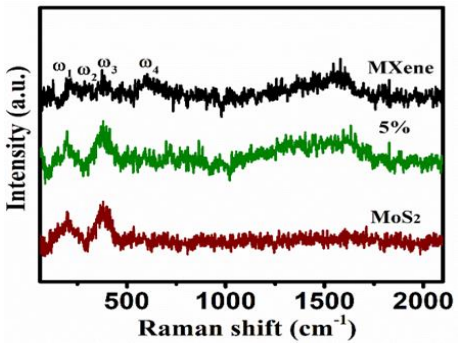

Fig. 2. Raman spectra of MXene, MoS2 and MoS2/MXene nanocomposite.

The morphology and architecture of sheet-like MXene, MoS_2 nanoflowers and MoS_2/MXene heterojunction were investigated by SEM, as shown Fig. 3. Clearly, MXene exhibits the typical accordion-shape multilayer structure with smooth surface after HF etching (Fig. 3a). And flower-like MoS_2 nanosheets with a size 100–200 nm is obtained in Fig. 3b. After hydrothermal reaction, petal-like MoS_2 nanosheets are uniformly distributed over the surface of layered MXene. Further characterized by TEM in Fig. 4, similarly, MoS_2 nanosheets evenly scattered on the surface of MXene layers (Fig. 4a), which is consistent with SEM results. Furthermore, HRTEM image (Fig. 4b) reveals the lattice spacing is slightly expanded to 0.65 nm, which can be indexed to the (002) plane of MoS_2.

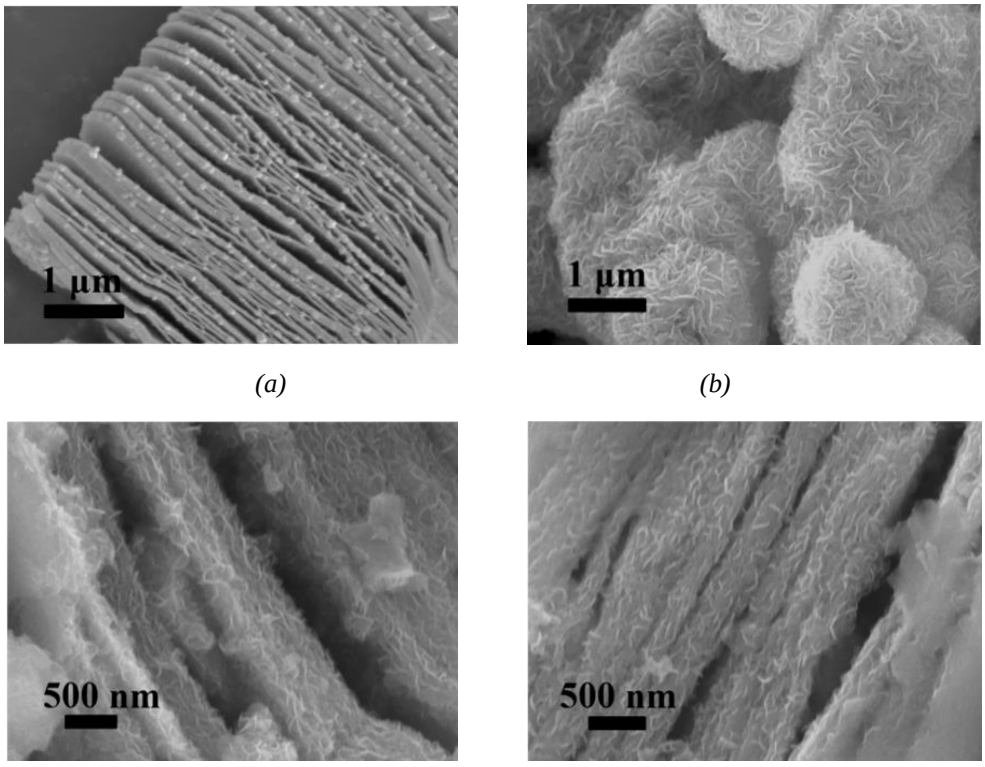

(a) *(b)*

(c) *(d)*

Fig. 3. SEM images of (a) MXene, (b) MoS_2, (c) MoS_2/MXene-5%; (d) MoS_2/MXene-15%.

Fig. 5 Friction coefficient of liquid paraffin contained with various oil additive; (b) Friction coefficient of liquid paraffin contained with different MoS_2/MXene composites additive; Variations of mean friction coefficient of paraffin with different additive (c) increasing load (2-6 N), (d) under diverse speeds (100-500 rpm).

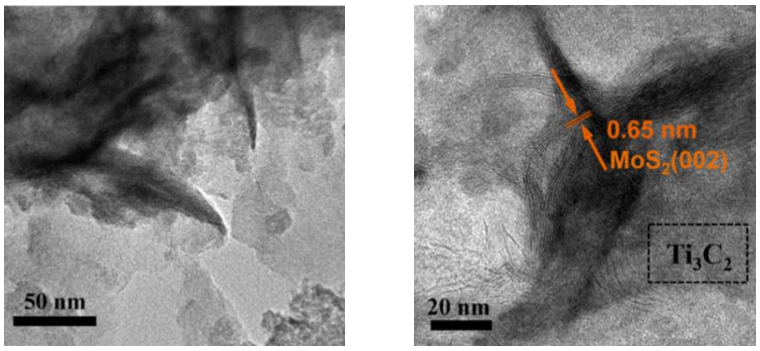

(a) *(b)*

Fig. 4. TEM images of MoS_2/MXene.

The tribological experiment of the as-synthesized sheet-like MXene, MoS_2 nanoflowers and MoS_2/MXene heterojunction contained with base oil were characterized by a ball-on-disk tribometer, and resulted in Fig. 5. Clearly, the average friction coefficient (COFs) of pure paraffin

exhibited higher friction coefficient of about 0.18 (Fig. 5a). In contrast, the COFs of pure paraffin contained with MXene, MoS_2 and MoS_2/MXene gradually decrease to 0.16, 0.14, and 0.11, respectively. Especially, the optimum adding amount of MoS_2/MXene in pure oil was 5%, and show the lowest COFs compared with other components, which could increase the lubrication effect of liquid paraffin significantly (Fig. 5b). Furthermore, 5%-MoS_2/MXene sample exhibits a steady variation curve of COFs and time (Fig. 5b inset), further indicating a stable friction-reducing process after the introduction of MoS_2/MXene. Further, the tribological behaviors of 5%-MoS_2/MXene sample were measured by applied loads (1-6 N) and rotating speeds (100-500 rpm) and the comparative experiments were performed using pure oil, MXene and MoS_2 as additives. Under the condition of increasing applied loads with steady speed (100 rpm), all friction curve of liquid paraffin contained with various additives show a similar trend. And the COFs of MoS_2/MXene was decreased remarkably to 0.10 at the applied load of 5N, resulted in Fig. 5c. Similarly, all curves of COFs were first decreased and then increased with the increasing of speeds, as shown Fig. 5d. And the lowest COFs of was appeared in 300 rpm, which is mainly attributed to the addition and synergistic effect of MoS_2 and MXene.

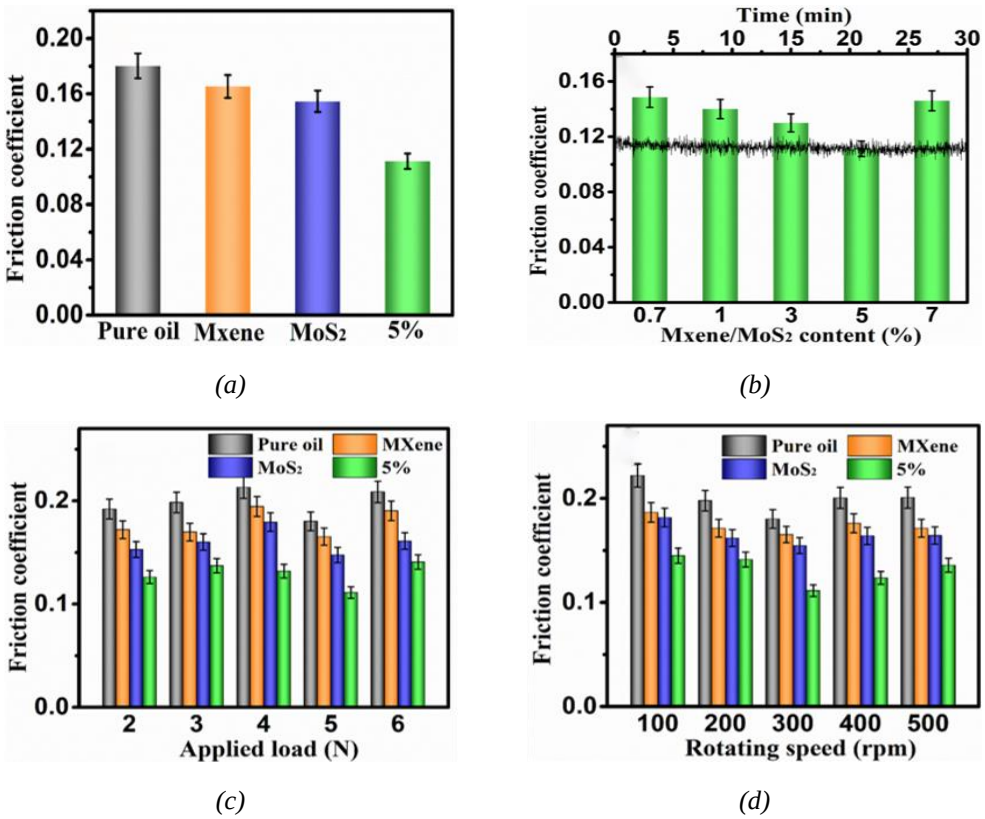

Fig. 5. Friction coefficient of liquid paraffin contained with various oil additive; (b) Friction coefficient of liquid paraffin contained with different MoS_2/MXene composites additive; Variations of mean friction coefficient of paraffin with different additive (c) increasing load (2-6 N), (d) under diverse speeds (100-500 rpm).

Further to explore the anti-wear property and lubricating mechanism of MoS_2/MXene in liquid paraffin during friction process, SEM and SMP analysis were employed to detect the

morphology of the worn steel surfaces. It can be clearly seen from SEM images (Fig. 6), the surface of steel disc lubricated by paraffin oil was serious wear, indicating poor anti-wear performance (Fig. 6a). On the contrary, the grinding crack on the surface of steel disc are gradually decreased, and no obvious wear furrows and cracks were observed with the introduction of different nano-additives (Fig. 6b-4d). Furthermore, 3D morphologies of friction interface were precisely detected by SMP technology, as shown Fig.7. Similarly, SMP results also indicate the morphology of the worn steel surfaces lubricated by MoS_2, MXene, and MoS_2/MXene in liquid paraffin were relatively smooth compared with that of pure paraffin. As expected, the wear scar lubricated by liquid paraffin is 7.549μm and 283.4μm(Fig.7a), while the wear scar lubricated by paraffin oil contained with MoS_2/MXene exhibits the minimum width of 1.391μm and depth of 206.3μm(Fig. 7d), which is also consistent with SEM results of wear scar. Additionally, all the above friction and wear results revealed MoS_2/MXene composite as an oil additive possessing superior friction-reduction and anti-wear.

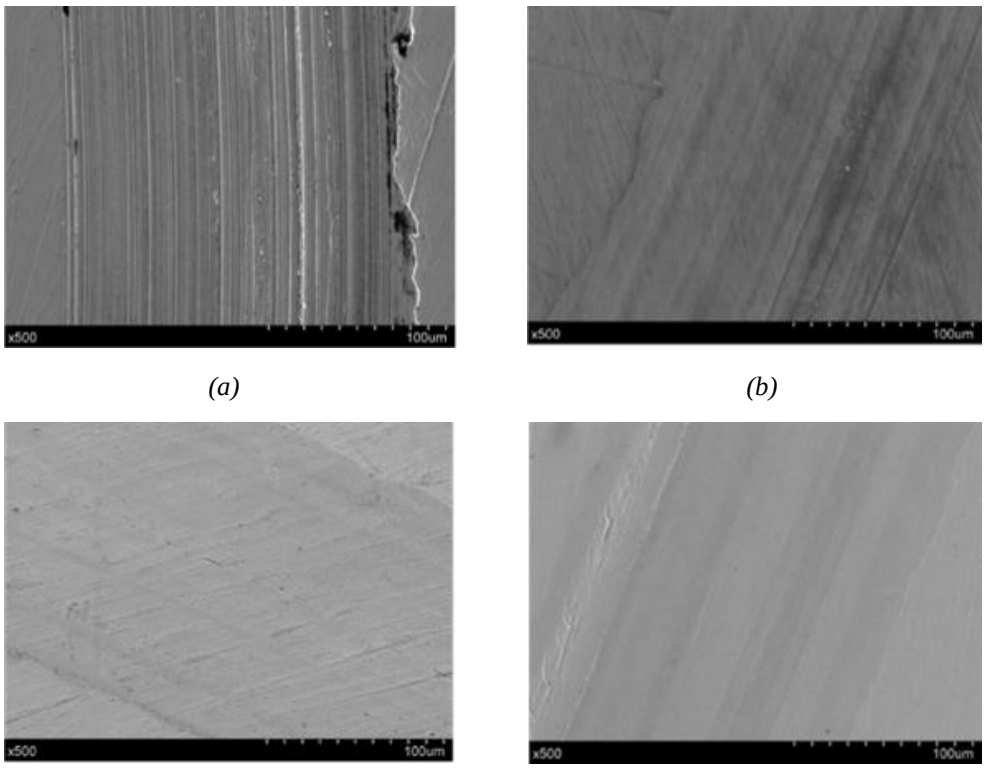

(a) *(b)*

(c) *(d)*

Fig. 6. SEM images of worn surfaces of (a) liquid paraffin, and liquid paraffin contained with (b) MXene; (c) MoS_2 and (d) MoS_2/MXene composites.

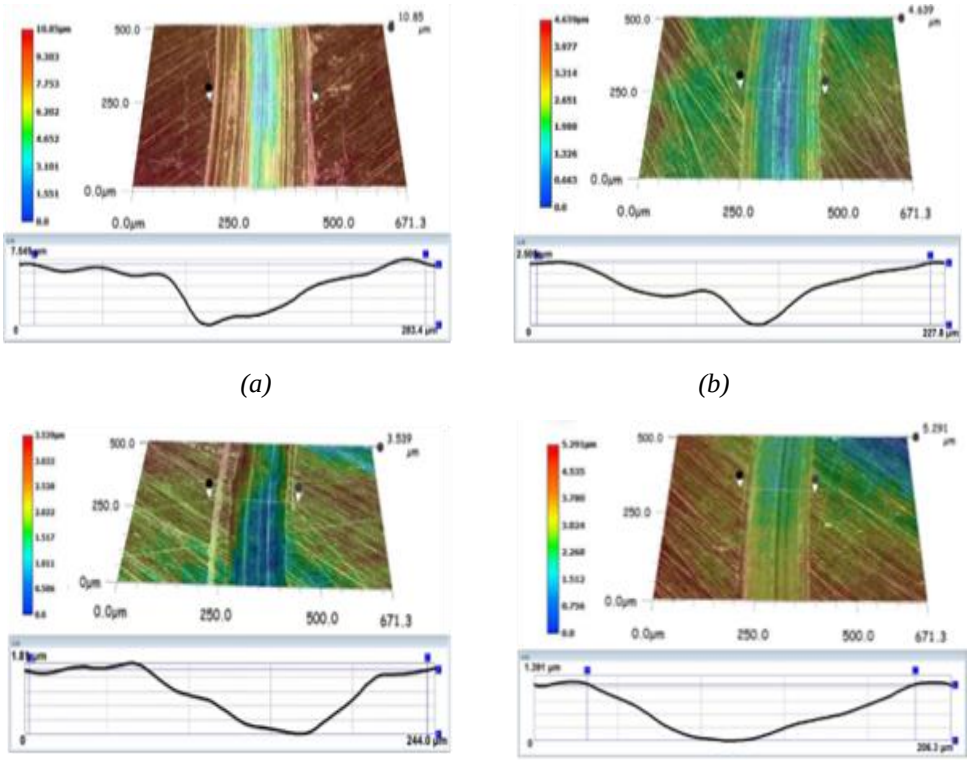

(a) *(b)*

(c) *(d)*

Fig.7 Noncontact three-dimensional images of worn surfaces of (a) liquid paraffin; and liquid paraffin contained with (b) MXene; (c) MoS_2 and (d) MoS_2/MXene composites.

EDX analysis of wear scar by was detect to investigate the change of chemical composition, and resulted Fig. 8.

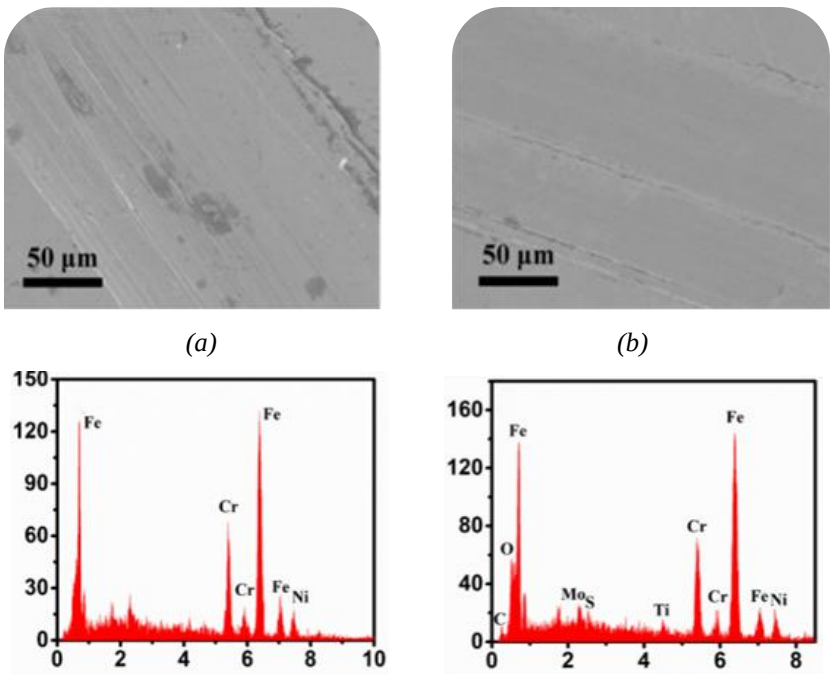

(a) *(b)*

(c) *(d)*

Fig. 8. SEM images and EDS of worn surfaces of (a, c) liquid paraffin and (b, d) MoS_2/MXene composites.

Obviously, the worn surfaces of pure paraffin is mainly consisted of Fe, Cr and Ni elements, while C, Ti, Mo, and S elements were obtained on the friction interface with the addition of MoS_2/MXene, which also reveals MoS_2/MXene nanocomposite could be transferred to the friction contact region and formed the tribo-film during the friction process.

According to the above tribological experimental results and related analysis by many recent reports, an underlying microscopic tribological mechanism was proposed and illustrated in Fig.9. The improved friction and wear properties of MoS_2/MXene composites are mainly attributed to their unique microstructure and the formation of tribo-film. Moreover, MoS_2/MXene can be adsorbed and deposited on the rubbing interfaces, which hindered the direct contact between the interfaces of steel disc and ball, and hence lower COFs and excellent antiwear ability have resulted. The conclusion on the wear mechanism of the composite by the debris topography analysis is coincident to that of the SEM analysis on the worn surface.

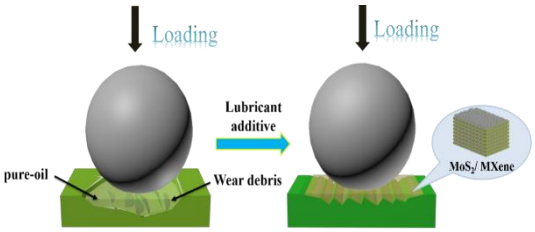

Fig. 9. The tribological mechanism of MoS_2/MXene additive in liquid paraffin.

4. Conclusions

Novel MXenes/MoS_2 heterojunction of flower-like MoS_2 decorated sheet-like MXenes were successfully constructed and synthesized by one-step hydrothermal approach in the presence of MXenes, which was applied directly as a novel lubrication additive for tribological studies of liquid paraffin. The characterization results indicate flower-like MoS_2 nanosheets evenly scattered on the surface of MXene layers. Furthermore, the tribological behaviour of MXenes/MoS_2 heterojunction in liquid paraffin were extensively examined a ball-on-disk tribometer, which indicate the friction and wear was significant decreased with introduction of MXenes/MoS_2 heterojunction. Especially, 5%-MXenes/MoS_2-paraffin samples show the lowest friction coefficient (~0.10). These results distinctly demonstrated MXenes/MoS_2 heterojunction as lubricant additives in liquid paraffin exhibited superior antifriction and wear resistant, would be beneficial for the design of novel nano-additives with 2D/2D structure for enhancing tribological properties.

Acknowledgements

Our research project was sponsored by National Natural Science Foundation of China (51672113, 21975110 and 21972058) , Natural Science Foundation of Jiangsu Province (BK20201424) and Primary Research & Development Plan(social development project) of Zhenjiang (SH2019016).

References

[1] Y. F. Zuo, J. Mei, X. A. Zhang, C. H. T. Lee, IEEE Trans. Power Electron. **36**, 716 (2021).

[2] W. T. Zhu, L. C. Guo, L. B. Shi, Z. B. Cai, Q. L. Li, Q. Y. Liu, W. J. Wang, Wear **398**, 79 (2018).

[3] G. Y. Pan, X. M. Zhang, P. Liu, L. Chen, J. Vib. Control., 1077546320959517 (2020).

[4] M. J. Zhang, B. B. Chen, Z. Dong, S. Wang, X. Li, Y. H. Jia, F. Y. Yan, Polym. Compos. **41**, 3768 (2020).

[5] R. Rattan, J. Bijwe, Tribol. Lett. **67**, 36 (2019).

[6] H. Shi, S. Du, C. Sun, C. Song, Z. Yang, Y. Zhang, Materials **12**, 45 (2019).

[7] H. Mishina, J. JPN. Soc. Tribol. **57**, 303 (2012).

[8] M. Umashankar, K. Annamalai, Mater. Today. **4**, 9141 (2017).

[9] R. Xia, X. Wang, B. Li, X. Wei, Z. Yang, Math Probl. Eng. **2019**, 4191570 (2019).

[10] J. Teng, H. Li, G. Chen, J. Cent. South Univ. **22**, 2875 (2015).

[11] C. Y. Min, Z. B. He, H. J. Song, D. D. Liu, W. Jia, J. M. Qian, Y. H. Jin, L. Guo, Appl Sci-Basel. **9**, 170 (2019).

[12] H. J. Song, Z. Q. Wang, J. Yang, Appl. Phy. A-Mater. **122**, 933 (2016).

[13] Y. Y. Wu, W. C. Tsui, T. C. Liu, Wear **262**, 819 (2007).

[14] J. Khedkar, I. Negulescu, E. I. Meletis, Wear **252**, 361 (2002).

[15] A. D. Moghadam, E. Omrani, P. L. Menezes, P. K. Rohatgi, Composites Part B **77**, 402 (2015).

[16] Z. Y. Zhang, Y. T. Zhao, C. L. Wang, R. Tao, Z. fang, Y. Sun, X. Z. Kai, Mat Sci Eng A-Struct. **788**, 139590 (2020).

[17] M. J. Zhang, B. B. Chen, Z. Dong, S. Wang, X. Li, Y. H. Jia, F. Y. Yan, Polym. Compos. **41**, 3768 (2020).

[18] W. W. Song, X. J. Xu, S. R. Liu, J. F. Pu, H. F. Wang, Adv. Compos Lett. **29**, 2633366X20927025 (2020).

[19] X. H. Jia, J. Huang, Y. Li, J. Yang, H. J. Song, Appl. Surf. Sci. **494**, 430 (2019).

[20] Y. M. Zeng, F. He, L. N. Si, Y. J. Wang, Q. Wang, Mater. Res. Express **6**, 1150b4 (2019).

[21] B. B. Chen, Y. H. Jia, M. J. Zhang, H. Y. Liang, X. Li, J. Yang, F. Y. Yan, C. S. Li, Composites, Part A **122**, 85 (2019).

[22] B. B. Chen, X. Li, Y. H. Jia, L. Xu, H. Y. Liang, X. F. Li, J. Yang, C. S. Li, F. Y. Yan, Compos. Part A Appl. Sci. Manuf. **115**, 157 (2018).

[23] J. Xu, H. Tang, Y. Chu, C. Li, Rsc Adv. **5**, 48492 (2015).

[24] X. Li, Z. Cao, Z. Zhang, H. Dang, Appl. Surf. Sci. **252**, 7856 (2006).

[25] L. Rapoport, V. Leshchinsky, I. Lapsker, Y. Volovik, O. Nepomnyashchy, M. Lvovsky, R. Popovitz-Biro, Y. Feldman, R. Tenne, Wear **255**, 785 (2003).

[26] J. Xu, H. Tang, G. Tang, C. Li, Chalcogenide Lett. **11**, 265 (2014).

[27] X. J. Hua, J. G. Sun, P. Y. Zhang, K. Liu, R. Wang, J. H. Ji, Y. H. Fu, J Tribol-T Asme. **138**, 031302 (2016).

[28] Y. Jiang, K. Shi, H. Tang, Y. Wang, Surf. Coat. Tech. **375**, 334 (2019).

[29] G. Li, C. Li, H. Tang, K. Cao, J. Chen, F. Wang, Y. Jin, J. Alloys Compd. **501**, 275 (2010).

[30] G. Tang, F. Zhang, J. Xu, Micro Nano Lett. **14**, 416 (2019).

[31] M. S. Zhang, B. B. Chen, J. Yang, H. M. Zhang, Q. Zhang, H. Tang, C. S. Li, RSC Adv. **5**, 89682 (2015).
[32] R. Zhou, Z. P. Tong, G. F. Sun, Z. H. Ni, W. Zhang, Lasers Eng. **41**, 1 (2018).
[33] J. Xu, H. Tang, Q. Shi, C. Li, Chalcogenide Lett. **12**, 1 (2015).
[34] B. B. Chen, M. J. Zhang, X. Li, Z. Dong, Y. H. Jia, C. S. Li, Prog. Org. Coat. **147**, 105767 (2020).
[35] W. Song, P. Chen, J. C. Yan, W. S. Zhu, H. B. Ji, ACS Appl. Mater. Interfaces **12**, 29737 (2020).
[36] C. Prasad, X. F. Yang, Q. Q. Liu, H. Tang, A. Rammohan, S. Zulfiqar, G. V. Zyryanov, S. Shah, J. Ind. Eng. Chem. **85**, 1 (2020).
[37] D. Q. Li, X. F. Chen, P. Xiang, H. Y. Du, B. B. Xiao, Appl. Surf. Sci. **501**, 144221 (2020).
[38] D. W. Rao, L. Y. Zhang, Y. H. Wang, Z. S. Meng, X. Y. Qian, J. H. Liu, X. Q. Shen, G. J. Qiao, R. F. Lu, J. Phys. Chem. C. **121**, 11047 (2017).
[39] X. H. Zhang, M. Q. Xue, X. H. Yang, Z. P. Wang, G. S. Luo, Z. D. Huang, X. L. Sui, C. S. Li, RSC Adv. **5**, 2762 (2015).
[40] A. Mukherji, L. Saikia, R. Srivastava, Chem. Eng. J. **373**, 1233 (2019).
[41] S. Bolar, S. Shit, J. S. Kumar, N. C. Murmu, R. S. Ganesh, H. Inokawa, T. Kuila, Appl. Catal. B-Env. **254**, 432 (2019).
[42] Y. Liao, J. Qian, G. Xie, Q. Han, W. Q. Dang, Y. S. Wang, L. L. Lv, S. Zhao, L. Luo, W. Zhang, H. Y. Jiang, J. W. Tang, Appl Catal B-Environ. **273**, 119054 (2020).
[43] Y. L. Sun, Y. Sun, X. Meng, Y. Gao, Y. Dall'Agnese, G. Chen, C. Dall'Agnese, X. F. Wang, Catal. Sci. Technol. **9**, 310 (2019).
[44] W. Y. Yuan, L. F. Cheng, Y. R. An, S. L. Lv, H. Wu, X. L. Fan, Y. N. Zhang, X. H. Guo, J. W. Tang, Adv. Sci. **5**, 1700870 (2018).